Influence of two different representations of the *G*-matrix to the in-medium nucleon-nucleon cross sections*

LUO Pei-Yan(罗培燕)[1,2;1)] ZUO Wei(左维)[1] U. Lombardo[3]

1 (Institute of Modern Physics, CAS, Lanzhou 730000, China)
2 (Graduate University of Chinese Academy of Sciences, Beijing 100049, China)
3 (Dipartimento di Fisica, Universit di Catania, c.so Italia 57, I-95129 Catania, Italy)

Abstract We calculate the in-medium nucleon-nucleon scattering cross sections from the *G*-matrix using the Dirac-Brueckner-Hartree-Fock (DBHF) approach. And we investigate the influence of the different representations of the *G*-matrix to the cross sections, the difference of which is mainly from the different effective masses.

Key words DBHF, self-energy, representation

PACS 21.65.-f, 21.30.Fe

1 Introduction

The transport models, which are employed to describe the heavy ion collisions(HIC), are powerful approaches to reproduce the collective observable in HIC and probe the equation of state(EOS) of nuclear matter[1]. Those models, such as the quantum molecular dynamics (QMD) and Boltzmann-Uehling-Uhlenbeck (BUU) equation as well as their relativistic extensions (RBUU and RQMD), treat the nucleon mean fields and nucleon-nucleon scattering cross sections as the basic input ingredients. Up to now, most calculations of particle producing in nucleus-nucleus reaction are using the free cross sections or the approximations $\sigma^*_{\rm NN} = 0.8\sigma^{\rm free}_{\rm NN}$, $\sigma^*_{\rm NN}/\sigma^{\rm free}_{\rm NN} = (m^*/m)^2$ instead of the in-medium cross sections[2—4].

Many recent papers have devoted to the in-medium N-N scattering problem within different methods, such as the collectivistic Brueckner approach[5], and DBHF approach[6, 7]. Here we apply the DBHF approach which can successfully describe the saturation mechanism of the nuclear matter[8]. However, because of the uncertainty in determining the nucleon self-energy in DBHF approach, Horowitz and Serot [9] have developed a projection technique to project the *G*-matrix elements onto five covariant amplitudes. This set of five covariant amplitudes is not unique, which is corresponding to different representations. Adopting the two different representations (pseudo-scalar(ps) and complete pseudo-vector(pv) representations), we investigate the effects of these two representations to the total and differential cross sections in this paper.

2 Relativistic Brueckner approach

In the relativistic Brueckner approach, the essential point is using Dirac equation to describe the single-particle motion in the nuclear matter,

$$[\gamma_\mu \widetilde{k}^{*\mu} - \widetilde{M}^*]u_\lambda(k) = 0 \ , \qquad (1)$$

Received 8 July 2008

* Supported by National Natural Science Foundation of China (10575119, 10775061) and Asia-Link Project (CN/ASIA-LINK/008(94791)) of the European Commission

1) E-mail: luopeiyan@impcas.ac.cn

by introducing the reduced kinetic momentum $\widetilde{k}^{*\mu}=\frac{k^\mu+\mathrm{Re}\Sigma^\mu(k)}{1+\Sigma_v(k)}$ and the reduced effective mass $\widetilde{M}^*=\frac{M+\mathrm{Re}\Sigma_s(k)}{1+\Sigma_v(k)}$, the scalar Σ_s and vector (Σ_0, Σ_v) are the three components of the self-energy. The solution of the in-medium Dirac equation is

$$u_\lambda(k)=\sqrt{\frac{\widetilde{E}^*(\boldsymbol{k})+\widetilde{M}^*}{2\widetilde{M}^*}}\begin{pmatrix}1\\ \frac{2\lambda|\boldsymbol{k}|}{\widetilde{E}^*(\boldsymbol{k})+\widetilde{M}^*}\end{pmatrix}\chi_\lambda\ , \quad (2)$$

where $\widetilde{E}(\boldsymbol{k})=\sqrt{\boldsymbol{k}^2+\widetilde{M}^{*2}}$, χ_λ denotes a two-component Pauli spinor with $\chi=\pm\frac{1}{2}$. The normalization of Dirac spinor is $\widehat{u}_\lambda(k,k_\mathrm{F})u_\lambda(k,k_\mathrm{F})=1$. The basic quantity in DBHF approach is the G-matrix, satisfying the Thompson equation which is most easily solved in the two-nucleon center of mass (c.m.) frame[6, 10],

$$G(\boldsymbol{p},\boldsymbol{q},\boldsymbol{P})|_{\mathrm{c.m.}}=V(\boldsymbol{p},\boldsymbol{q})+\int\frac{\mathrm{d}^3\boldsymbol{k}}{(2\pi)^3}\frac{\widetilde{M}^{*2}}{\widetilde{E}^{*2}(\boldsymbol{k})}\times\frac{Q(\boldsymbol{k},\boldsymbol{P})}{2\widetilde{E}^*(\boldsymbol{q})-2\widetilde{E}^*(\boldsymbol{k})+\mathrm{i}\epsilon}G(\boldsymbol{k},\boldsymbol{q},\boldsymbol{P}),(3)$$

where $\boldsymbol{q}$, $\boldsymbol{k}$, $\boldsymbol{p}$ are the relative momenta of the initial, intermediate and final states, respectively, $\boldsymbol{P}$ is the total center of mass momentum. The starting energy in Eq. (3) is fixed to $\sqrt{s^*}=2\widetilde{E}^*(\boldsymbol{q})$. The Pauli operator Q, preventing the nucleons scattering onto occupied intermediate states, usually is replaced by an angle-averaged Pauli operator $\overline{Q}$ for simplicity. In order to get the the self-energy in rest frame from the G-matrix in c.m. frame, we need to construct the G-matrix in a covariant way using the ps and pv representations. Thus starting from reasonable initial values for every part of self-energy, one obtains the G-matrix by solving the in-medium Thompson equation in momentum space, then leading to a new set of values for self-energy which will be used in the next iteration. This procedure is continued until the convergence is achieved.

3 On-shell scattering cross sections

For on-shell nucleon nucleon interaction, there are only five independent G-matrix elements, one can directly calculate the cross sections from those elements[11] ($|\boldsymbol{p}|=|\boldsymbol{q}|$). The differential cross section is given as[7],

$$\mathrm{d}\sigma=\frac{(\widetilde{M}^*)^4}{s^*4\pi^2}|\widehat{G}(q,q,\theta)|^2\mathrm{d}\Omega \quad (4)$$

and

$$|\widehat{G}(q,q,\theta)|^2=\sum_{i=1}^{6}\beta_i\Big[\Big(\sum_J\frac{2J+1}{4\pi}\mathrm{d}^J_{\lambda_i\lambda_i'}(\theta)\mathrm{Re}G_i^J(q,q)\Big)^2+\Big(\sum_J\frac{2J+1}{4\pi}\mathrm{d}^J_{\lambda_i\lambda_i'}(\theta)\mathrm{Im}G_i^J(q,q)\Big)^2\Big]. \quad (5)$$

The weighting factors $\beta_i=2$, $i=1,\cdots,4$, and $\beta_5=\beta_6=4$ arise from the sum over all helicity states. Using the orthogonality relation for the rotation matrices,

$$\int\mathrm{d}\cos(\theta)d^J_{\lambda_i\lambda_i'}(\theta)d^{J'}_{\lambda_i\lambda_i'}(\theta)=\frac{2}{2J+1}\delta_{JJ'}\ . \quad (6)$$

We can get the total cross section

$$\sigma_{\mathrm{tot}}=\int\mathrm{d}\Omega\frac{(\widetilde{M}^*)^4}{s^*4\pi^2}|\widehat{G}(q,q,\theta)|^2=\frac{(\widetilde{M}^*)^4}{s^*4\pi^2}\sum_{i=1}^{6}\beta_i\times\sum_J\frac{2J+1}{4\pi}\big([\mathrm{Re}G_i^J(q,q)]^2+[\mathrm{Im}G_i^j(q,q)]^2]\big) \quad (7)$$

where $G_i^J=0.5(G_i^{J,I=0}+G_i^{J,I=1})$ and $G_i^J=G_i^{J,I=1}$ are the average neutron-proton and proton-proton(same as neutron-neutron) on-shell G-matrix elements respectively.

4 Numerical results and conclusions

In this section we present the numerical results to investigate the influence of these two representations of the G-matrix to the cross sections. For the bare nucleon-nucleon potential we adopt Bonn A potential. First we calculate the G-matrix in the c.m. frame of the two interacting nucleons, i.e., we use Eq. (3) with $\boldsymbol{P}=0$. The relative momentum q is related to the kinetic energy of the incident nucleon in the "laboratory system" $E_{\mathrm{lab}}=2q^2/m$, in which the other nucleon is at rest. In the following we consider the in-medium cross sections at three different Fermi momenta k_F =1.1, 1.39 and 1.75 fm^{-1}, corresponding to densities ρ=0.09, 0.18 and 0.36 fm^{-3} with the nuclear saturation density ρ_0 =0.18 fm^{-3}.

In Fig. 1, the differential np cross sections at different densities are shown at E_{lab} =40, 90 and 250 MeV with the two representations of the G-matrix for comparison. The vacuum results are also presented. With the ps presentation, the np differential cross sections tend to decrease with the increasing

of density at fixed laboratory energy and also decrease with the increasing of laboratory energy at fixed density. With the pv presentation, the results are similar except that at the density $\frac{1}{2}\rho_0$ the lines are greatly enhanced at low energies. We also present the pp differential cross sections in Fig. 2, the results of which are much more isotropic compared with Fig. 1. At last, we give the results of the np and pp total cross

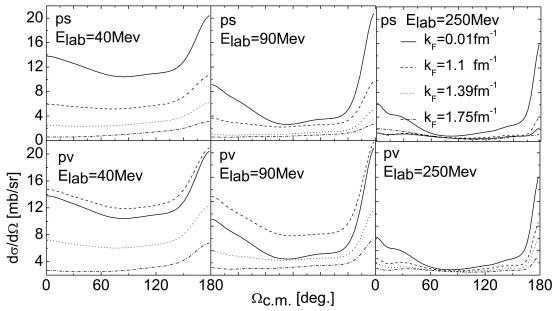

Fig. 1. In-medium np differential cross sections obtained at various laboratory energies and densities are functions of angles. The upper three with ps representation and the lower three with pv representation.

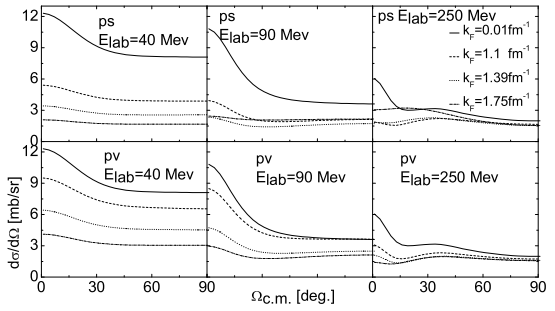

Fig. 2. The same as Fig. 1, but for in-medium pp differential cross sections.

sections as functions of laboratory energies in Fig. 3 and Fig. 4. For np channel, the total cross sections with ps representation decrease with the increasing of density, while with pv representation there is a bump at moderate energy and density $\frac{1}{2}\rho_0$. But for pp channel, the bump is not evident. For every figure, the cross sections with pv representation change with density or laboratory energy more smoothly than those with ps representation, which is mainly due to the difference of effective masses with two representations through the factor of $\widetilde{M}^{*4}/(4\pi^2 s^*)$ in Eq. (7). And in this paper, at different Fermi momenta $k_{\rm F}$ = 1.1, 1.39, 1.75 fm^{-1}, we get $\widetilde{M}^*$ =592.4, 479.2, 339.0 MeV with ps representation , while $\widetilde{M}^*$=766.6, 660.2, 527.6 MeV with pv representation.

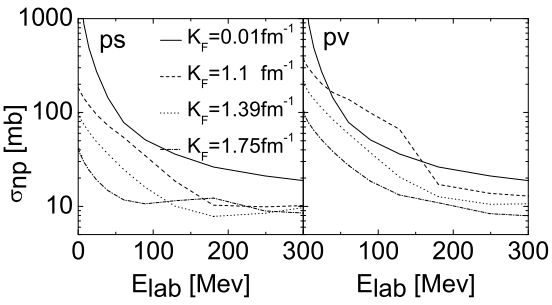

Fig. 3. In-medium np total cross sections are functions of laboratory energies, left one with ps representation, right one with pv representation.

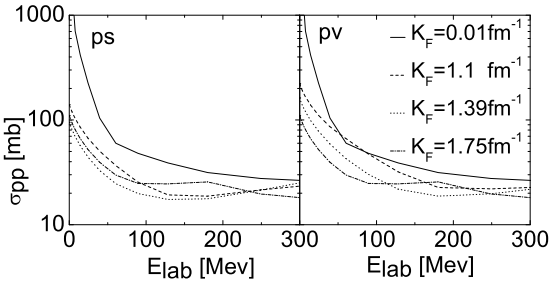

Fig. 4. In-medium pp total cross sections with two representations, same as Fig. 3.

References

1 LI B A, Sustich A. Phys. Rev. Lett., 1999, **82**: 5004
2 George F.Bertsch, Gerald E. Brown, Volker Koch, LI Bao-An. Nucl. Phys. A, 1988, **490**: 745
3 Declan Persram, Charles Gale. Phys. Rev. C, 2002, **65**: 064611
4 LI Bao-An, CHEN Lie-We. Phys. Rev. C, 2005, **72**: 064611
5 Giansiracusa G, Lombardo U, Sandulescu N. Phys. Rev. C, 1996, **53**: R1478
6 LI G Q, Machleidt R. Phys. Rev. C, 1993, **48**: 1702
7 Fuchs C, Amand Faessler, El-Shabshiry M. Phys. Rev. C, 2001, **64**: 024003
8 Gross-Boelting T, Fuchs C, Amand Faessler. Nucl. Phys. A, 1999, **648**: 105
9 Horowitz C J, Serot B D. Nucl. Phys. A, 1987, **464**: 613
10 Fuchs C. arXiv: nucl-th/ 0309003
11 ter Haar B, Malfliet R. Phys. Rev. C, 1987, **36**: 1611